Surface Wear Resistant of 2024-T351 Aluminum Alloy under Cyclic Load of Spherical Rolling Bodies

Anatoly Gormakov[1,a*] and Aleksey Golikov[1,b]

[1]Tomsk Polytechnic University, 30 Lenin Avenue, 634050 Tomsk, Russia

[a]gormakov@tpu.ru, [b]nilis@tpu.ru

Abstract. The paper presents the experimental results of the possible use of the type 2024-T351 aluminum alloy for manufacturing the ball bearing rings of the rotary support system of the calibration equipment for magnetometric inclinometers. Non-magnetic materials for ball bearing manufacturing are reviewed. The description is given to the test equipment and procedures. The experimental results demonstrate that the type 2024-T351 aluminum alloy can be used for manufacturing a tailor-made ball bearing of the rotary support system. Stresses arising in the contact area do not exceed the allowable values of $\sigma_{max} \leq (0.3\text{–}0.5)\sigma_{0,2}$.

Introduction

In a number of devices and installations, their constructions should produce no distortion of the geomagnetic field and therefore must be made from non-magnetic materials. These comprise the calibration equipment for magnetometric borehole inclinometers.

The up-to-date and prospective installations of this designation reproduce the spatial orientation of borehole inclinometers by azimuth and sighting (apsidal) angles between 0 degrees to 360 degrees and zenith angle between 0 degrees to ±180 degrees, both with an error not over ±1'. The installation construction provides calibration of the borehole inclinometers and sensing units with the parameters not exceeding 100 mm in diameter, 100 kg in weight and 4 m in length [1]. Their lifetime is not less than 10 years. In order to prevent the structural deformations during the calibration process, the bearing members are provided with the appropriate rigidity, and their mass/volume parameters should be minimized.

Pan and tilt rotary system UNP-3, the three-dimensional view of which is given in Fig. 1, is a contemporary representative of such installations. At the inclinometer weight not over 100 kg, azimuthal rotation of the UNP-3 is performed easily and slowly.

Fig. 1. Pan and tilt rotary system UNP-3

Ball Bearing Review

The rotary support system of the pan and tilt rotary system UNP-3 are mounted to the pedestal 1 (Fig. 1). The load on the rotary support may vary from 500 to 580 kg. Under such loading, the friction torque of slider bearings made from conventional antifriction materials, achieves excessive values causing significant difficulties while in operation. Moreover, scuffing and severe wear of material occur on the bearing working surface resulting in the loss of the instrument accuracy.

Gas-lubricated slider bearings (gasostatic bearings) allow a user to considerably reduce the friction. However, this rather complicates the construction of the installation and, as a consequence, increases its value and operating costs.

In the last decades, the development of new materials for slider bearings has attracted much attention from research teams of the world engaged in triboengineering materials. Owing to the lack of tin and lead, aluminum alloys and aluminum-based compositions are utilized in manufacturing slider bearings.

Aluminum alloys possess the proper antifriction properties, high thermal conductivity, corrosion resistance in oil media, and demonstrate quite satisfactory processing behavior. Previous research [2–12] is devoted to triboengineering properties of aluminum-based alloys, enhancement of strength and wear resistance of the surface structures. New alloys, composites, coatings and specific methods of the surface treatment are being developed today in order to accomplish these goals. However, higher friction torques in slider bearings limit the scope of their application.

Search for non-magnetic ball bearings manufactured in Russia and abroad has produced no positive results. In Russia, ball bearing plants are not involved in manufacture of non-magnetic bearings which are able to withstand mean and high loads. Execution of orders on the single or small-lot production of a big ball bearing tailored to individual customer requirements and made from non-traditional, non-magnetic materials (aluminum alloys, ceramics, steels, *etc*.) is economically unprofitable for ball bearing plants.

Franke Company (Germany) [13] supplies a wide variety of non-magnetic ball bearings made from aluminum alloy. The diameter of the inner and outer rings is respectively 1400 and 1600 mm. These bearings operate at temperatures ranging from –30 to 80 ºC and take both radial and axial loads. Franke, however, does not ensure the required stability of the rotary axis of the aluminum-made upper (moving) ring under the indicated loads and lifetime.

The implementation of requirements for the high contact rigidity of the structural elements of the pan and tilt rotary system UNP-3 and the wear resistance of friction assemblies while meeting the requirements for non-magnetization of materials is rather a complicated matter. In solving this problem, it is important to provide the optimum ratio between the price and quality.

This resulted in decision to develop and manufacture a tailor-made bearing for the rotary support intended for pan and tilt rotary systems.

Ball Bearing Prototype. The following aspects are integrated into the design of the bearing for the rotary support system:

1) materials of the ball bearing elements are non-magnetic that precludes the application of conventional ball bearing steels;

2) bearing elements are subjected to cyclic loads and must possess sufficient strength, rigidity and wear resistance;

3) the load on the bearing assembly varies between 500–580 kg;

4) the operational life of the ball bearing should be not less than 10 years throughout a year of its every day operation;

5) within one working day, the moving ring of the ball bearing executes about 20 rotations;

6) rotation speed is not over 5 rpm. The bearing is subjected to a static load for the most of its operating time;

7) an intolerably high friction torque occurs under the indicated static load in the slider bearing;

8) the use of gasostatic bearings complicates the construction and increases operating costs;

9) industrial lot production in Russia produces ball bearings with 32 mm in diameter, whereas abroad the diameter achieves 57 mm;

10) Franke Company does not ensure the required stability of the rotary axis of the aluminum-made outer ring of the type UNP-3 installations under the specified loads and operational life. Therefore, manufacturing of the tailor-made ball bearing becomes highly relevant. The cross sectional view of such bearing is shown in Fig. 2.
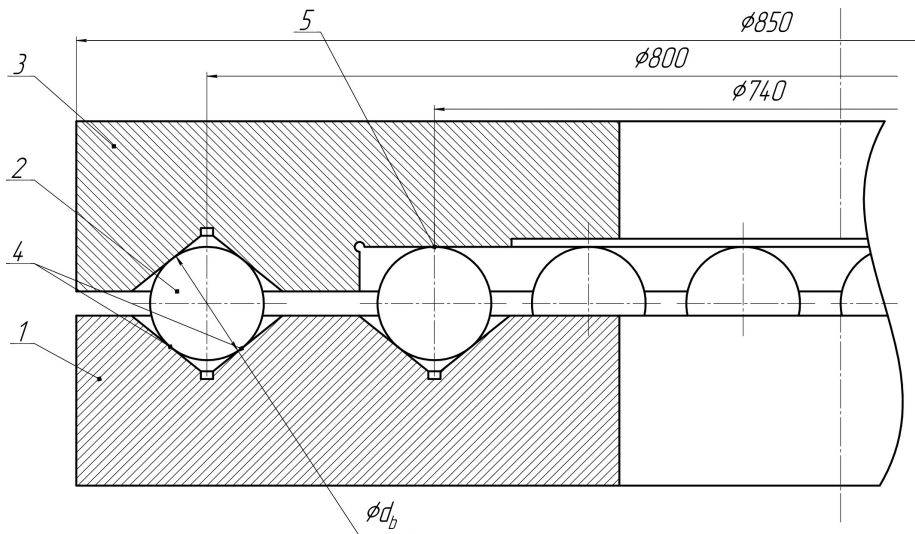

Fig. 2. Cross-sectional view of the tailor-made ball bearing

The lower ring *1* and the upper ring *2* of the double-row bearing are made from the type 2024-T351 aluminum alloy. The balls *2* can be made either from the type 40KhNYu-VI non-magnetic precision alloy (39–41% Cr, 3.3–3.8% Al, less 0.6% Fe, 0.03%C, 0.1% Mn, 0.1%Si, 0.01% S, 0.01% P, rest Ni) or ceramics. A multi-row ball bearing can be used to reduce the load at the contact points *4* and *5* between balls *2* and bearing tracks of rings *1* and *3*. However, prior to manufacturing of such a bearing, it is necessary to study the wear resistance of materials which are not traditional for this purpose.

Ball Bearing Materials. Including bearings, the structural members of the installation should not exert any effect on sensitive elements of the instrument to be tested. Non-magnetic materials include paramagnetics ($\mu<1.000021$), diamagnetics ($\mu = -0.9999904$), weakly ferromagnetic materials ($\mu < 1.05$) and also polymers, glass and ceramics.

Non-magnetic materials based on nonferrous metals usually possess lower magnetic permeability than non-magnetic steels and irons. They are easily processed by machining and pressure shaping, but their mechanical properties are not always satisfactory.

In steels and irons, non-magnetization is provided by the austenite structure created in them through the alloying process. Non-magnetic steels are produced in the form of sheets, wires, and straps. Non-magnetic chrome-nickel steels possess the best processing characteristics. Typical composition and properties of non-magnetic steel with high corrosion resistance include up to 0.12% C, 0.8% Si, 1–2% Mn, 17–19% Cr and 11–13% Ni; 1.05–1.2 magnetic permeability; 500–600 mN/m^2 (50–60 kgf/mm^2) tensile strength and 40–50% failure elongation.

Elements having a complex configuration and not responsible for high bearing loads are usually made from cheaper non-magnetic irons. The most widespread iron composition is 2.6–3.2% C, 5–7.5% Mn, 9–12% Ni, 2.5–3.5% Si and up to 1.1% P. Their magnetic permeability ranges between 1.03–1.06 and they are easily processed by machining.

Hadfield steel is a wear-resistant (resistant to abrasion) steel with a high manganese (11–14%) and carbon (0.9–1.3%) content. Its wear resistance is well demonstrated under high pressures or impact loads. Mold castings of the types A128, J91109 and J91139 steels are widely used in industry. After 800–900 °C tempering the steel becomes non-magnetic. After the steel work hardening, the Rockwell hardness number achieves 35–40. However, during the operation under load, some parts of the bearing elements become magnetized in stress zones. The limitations of Hadfield steel should also include its bad machining and, therefore it cannot be used in our experiment.

Non-magnetic aluminum alloys are characterized by the low density and rather high relative strength. The type 2024-T351 tempered and aged alloy relate to non-magnetic aluminum alloys. Since bearing elements are subjected to cyclic loads, they should possess high hardness and wear resistance and provide the lowest friction torque. The properties of some of non-magnetic materials recommended for manufacturing the structural members of rotary supports are summarized in Table 1.

In order to ensure that pan and tilt rotary systems are non-magnetized, developers are forced to utilize a number of non-traditional materials in manufacturing members for bearing assemblies and driving mechanisms. The application of these materials is only possible after the computer simulation and experimental research.

The analysis of and experimental studies on the stress state of the working surfaces of bearings made from 2024-T351 aluminum alloy, were carried out under the guidance and with the direct participation of the authors.

Table 1. Main parameters of non-magnetic materials for tailor-made ball bearing elements

Materials	Composition	Elasticity modulus [GPa]	Strength limit [MPa]	Hardness	Density [g/cm^3]	Rel. permeability	Iron impurities [%]
Non-magnetic materials							
Ceramics	Al_2O_3	382	4000 (CS)[*]	–	–	<1.01	–
Ceramics	Si_3N_4	450-520	3500 (CS)	75–80 HRC	3.2	<1.01	–
Al alloy	2024-T351	72	440-460	120-130 HB	2.78	<1.01	<0.5
Steel	40KhNYu-VI	196	1300	3200	–	–	–
Aged bronze	CuBe2Ni(Co) (solid state)	130	900	350–400 HV	8.2	<1.01	0.15
	CuBe2NiTi (solid state)	141	900	350–400 HV	8.3	<1.01	–

[*]Compressive strength

The experimental prototype of the rotary support was designed and manufactured from 2024-T351 aluminum alloy to experimentally determine the operational life of the ball bearing.

Rotary Support Prototype

The profile of the rotary support prototype is presented in Fig. 3. The bearing rings *1* and *3* are manufactured from the type 2024-T351 aluminum alloy.
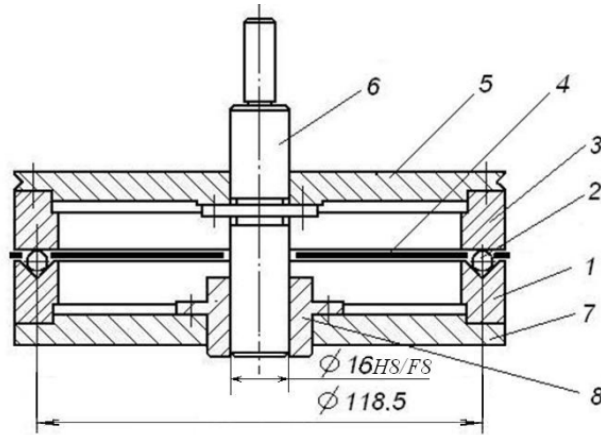
Fig. 3. Profile of the rotary support prototype

The bearing consists of 36 balls *2* having 5.59 mm diameter and they are made from the type 40KhNYu-VI non-magnetic alloy intended for instrument bearings. The ball bearing cage *4* is made from laminated fabric. The upper ring *3* is mounted to the sheave *5*. The lower ring *1* is provided with a groove having an apex angle of 90 degrees. The bearing track of the upper ring *3* is in the form of a plane. The load distribution covers three contact points between the ball and the ring plane. Such an axial bearing does not ensure centering of the axis of rotation, and thus is added with a radial slider bearing. The latter is formed by the steel shaft *6* rigidly fixed to the sheave *5* and bronze insert *8* attached to the base plate *7*.

As can be seen from Fig. 3, the contact area between the ball *2* and the upper ring *3* is the most loaded. The load distribution on the lower ring *1* falls into two contact points of the ball *2*. Let us estimate the stress within the contact zone between the ball and the upper ring. The maximum load on the bearing is 350 N. In the prototype, 36 balls are uniformly distributed over the circle with the diameter of 118.5 mm. The contact point load of the upper ring is 9.72 N. See Table 1 for the main parameters of non-magnetic materials for manufacturing elements of the tailor-made ball bearing.

Contact Stress Analysis

In the case of the initial contact between the ball and the plane of the upper ring, the contact stress is calculated by the Hertz equation:

$$\sigma_{max} = 0.388 \cdot \sqrt[3]{\frac{P \cdot E_r^2}{R_I^2}}. \tag{1}$$

The reduced modulus of elasticity of the couple of contacting materials is calculated as E_r $= E_r = \frac{2E_1 E_2}{E_1 + E_2} = 105.31$ GPa. The reduced radius is $\frac{1}{R_r} = \frac{1}{R_1} \pm \frac{1}{R_2}$, where R_1 is the ball radius; R_2 is the track groove radius; plus and minus signs indicate the outer and the inner contact areas, respectively. At the ball/plane contact (initial running period), the reduced radius R_r equals the radius of the ball, *i.e.* $R_1 = 5.59/2 = 2.795$ mm; $R_2 = \infty$.

Let us calculate the stress during the initial operation under the total bearing load of $P_\Sigma = 11.08$ N. When the number of balls is 36 and the variation factor is $k = 0.8$ for the load distribution, the contact point load is $P = P_\Sigma / k \cdot n = 11.08/0.8 \cdot 36 = 0.385$ N.

$$\sigma_{max} = 0.388 \cdot \sqrt[3]{\frac{P \cdot E_r^2}{R_I^2}}. \tag{2}$$

According to Table 2, in the case of the initial ball/plane contact, the stress substantially exceeds the value of $\sigma_{0.2} = 320$ MPa allowable for 2024-T351 aluminum alloy. In the case of the contact point load $P = 11.84$ N, the stress value also exceeds the value of 900 MPa allowable for 40KhNYu-VI alloy. And only the load of $P = 0.382$ N in the contact zone does not exceed the yield stress.

The ball distribution in the bearing rings without the ball bearing cage increases their number from 36 to 60. In this case, the contact point load decreases down to 0.250 N and the maximum stress σ_{max} achieves 272 MPa.

Table 2. Stress analysis results at ball/plane contact point

Total load P_{Σ} on rotary support system, N	341.27	106.89	39.32	11.08
Contact point load P of upper ring, N, ($n = 36$)	11.84	3.71	1.37	0.382
Stress $\sigma_{max,}$ MPa at $R_2 = \infty$ (prior to running)	993	672	484.2	316
Stress $\sigma_{max,}$ MPa at $R_2 = 2.895$ mm (after running)	105	70.49	48.5	33.6

During the bearing running, the track groove appears on the ring surface. The radius R_2 of the track groove approaches to the radius R_1 of the ball. At the same time, the contact area increases. The radius $R_2 = 2.895$ mm is relatively larger than the radius R_1 of the ball. In this case, the maximum stress in the contact point of the ball/concave surface can be obtained from

$$\sigma_{max} = 0.388 \cdot \sqrt[3]{\frac{P \cdot E_r^2 (R_2 - R_1)^2}{(R_I \cdot R_2)^2}}. \tag{3}$$

The results of the contact stress analysis after the bearing running are summarized in Table 2. As can be seen from this table, the maximum stress values are considerably lower than the proportionality limit for 2024-T351 alloy at the radius values specified for rolling bodies. Thus, under the maximum load of $P_{\Sigma} = 341.27$ N, the maximum contact stress is $\sigma_{max} = 105$ MPa. This value equals $0.33 \cdot \sigma_{0.2}$, *i.e.* 35% of the proportionality limit. These findings reveal that under the selected contact point loads, the ball bearing made from 2024-T351 alloy, is operable.

Experimental

Experimental Setup. The experimental setup was designed and manufactured to test the possibility of using the 2024-T351 alloy as material for making bearing rings. The full view of this setup is presented in Fig. 4.
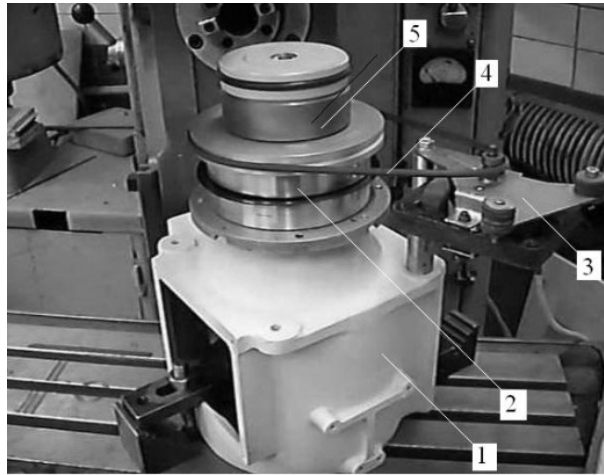
Fig. 4. Full view of experimental setup: 1 – pedestal; 2 – rotary support; 3 – driving mechanism;
4 – belt drive; 5 – steel disks (106.89 N load)

The lower (stationary) bearing ring and the driving mechanism of the upper ring are mounted to the pedestal. The rubber belt drive transmits the torque from the shaft of the driving mechanism to the sheave fixed to the upper ring. The belt drive effectually damps vibrations produced by the angular velocity of the driving mechanism. The pedestal is mounted and clamped to the milling-machine table. Several steel disks are used to provide the load.

Experimental Technique. The bearing running continued for a month, under the load and 100 rpm average rotation speed of the upper ring. The rotation speed was gradually increased with time, *i.e.* 1.13 kg after 380 min; 4.01 kg after 470 min; 10.9 kg after 320 min; and 34.8 kg after 1160 min.

The total running amounted to 2.330 minutes. At the average rotation speed of 100 rpm, the upper ring executed 244,000 revolutions. After running, a 240 h delay was performed under the static load of 34.8 kg.

Test Results. After the preliminary running at light loads, the formation of grooves is observed on the plane working surfaces of the bearing rings. The value of the groove radius approaches to that of the ball radius. Due to the increase in the ball/plane contact area, the contact stress decreases in several times and does not exceed the yield stress of the ring material.

During the experiment, the ring material is subjected to $8.8 \cdot 10^6$ loading cycles. The shape, geometry, and quality of the ring tracks formed by the end of the experiment are illustrated in Figures 5 and 6. The width and the height of the spherical groove of the upper ring is 1.119 mm and ~0.057 mm, respectively. Originally, precision turning is used to process the working surfaces of the rings. The accuracy degree is 10, the surface finish ranges between 5 and 25 μm.

During the bearing running, when the loaded balls roll in the groove, the crumpling and smoothing of the surface microroughness are followed by the material hardening. The ball in the lower ring contacts with two its surfaces, and the contact point load here is 0.707 times lower than that in the upper ring.

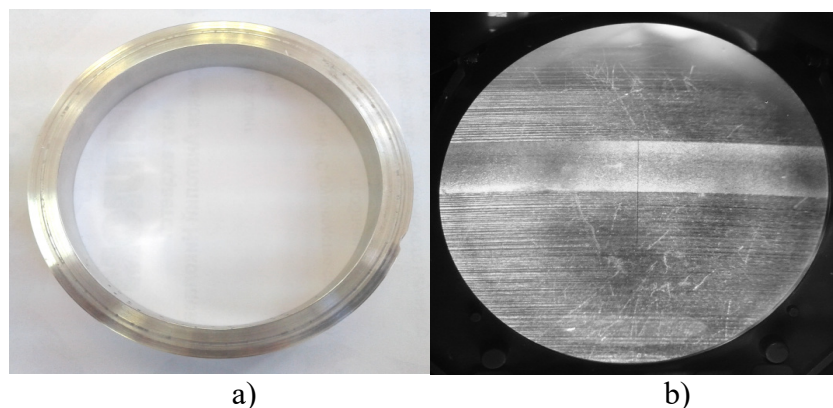a)   b)

Fig. 5. Upper ring tracks after testing: *a* – upper ring; *b* – spherical groove

A Kestrel non-contact measuring microscope and a MBS-10 microscope were used for precision contactless measurements and visual evaluation of the track surface quality at 5× magnification.
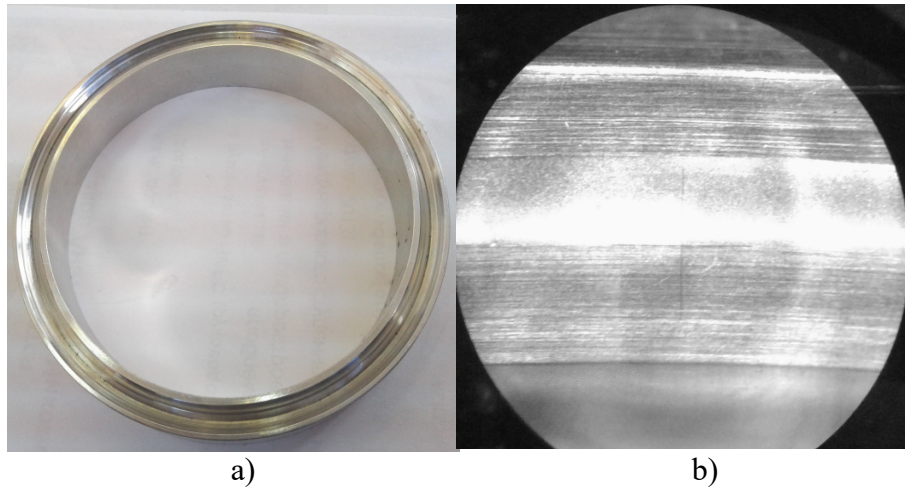

a)   b)

Fig. 6. Lower ring tracks after testing: a – lower ring; b – tracks

After $8.8 \cdot 10^6$ loading cycles, the lower ring is characterized by a perfect spherical surface formed in places of the ball rolling, as presented in Fig. 6b. The upper ring also acquires a spherical surface, however, with insignificant changes (coarse defects) in about 36 places, obviously caused by a 32 kg impact load. Later, in the course of running, these defects are smoothed, however, not fully.

Conclusions

It was found that during the bearing running, the radius values of the grooves and balls were almost similar, and the contact area increased. At the same time, the maximum stress in the contact area decreased down to values significantly lower than that of the yield stress of contacting materials. It was shown that increase in the number of balls (rolling bodies) also improved the durability of the ball bearing made from 2024-T351 alloy at gradual decrease in the contact point load. This can be achieved by the use of ball bearings either without a ball bearing cage or with the increased the number of track rows.

Assuming that the rotary support runs at 30 revolutions per day, it will perform 244.000 revolutions approximately for 22 years, throughout a year of every day operation. Such operational life will satisfy the requirements of every customer.

The results obtained showed that the type 2024-T351 alloy can be successfully used in manufacturing rings for a tailor-made bearing intended for the rotary support system. Stresses arising in the contact area will not exceed the allowable values of $\sigma_{max} \leq (0.3–0.5)\sigma_{0,2}$.

Acknowledgements

References

[1] Information on http://www.oskbp.ru/index.php?id=19

[2] H.B. Bhaskar and Abdul sharief, Tribological properties of aluminium 2024 alloy–beryl particulate MMC's, Bonfring International Journal of Industrial Engineering and Management Science 2(4) (2012) 143-147.

[3] A. Astarita, F. Rubino, P. Carlone, A. Squillace, On the improvement of AA2024 wear properties through the deposition of a cold-sprayed titanium coating article, Metals - Open Access Metallurgy Journal, 6(8) (2016) doi: 10.3390/met6080185.

[4] Yu. Golovin, V. Vasyukov, E. Isaeva, A. Kolmakov, R. Stolyarov, K. Tikhomirova, A. Tkachev, A. Shuklinov, Modification of aluminum antifriction alloys by carbon nanomaterials, Science+Business Media, Springer, 2011.

[5] J. Zhou, J. Li, S. Xu, S. Huang, X. Meng, J. Sheng, H. Zhang, Y. Sun, A. Feng, Improvement in fatigue properties of 2024-T351 aluminum alloy subjected to cryogenic treatment and laser peening, Surface and Coatings Technology 345 (2018) 31-39, doi:10.1016/j.surfcoat.2018.03.088

[6] M. Prudhomme, F. Billy, J. Alexis, G. Benoit, F.Hamon, C.Larignon, G.Odemer, C. Blanc, G.Hénaff, Effect of actual and accelerated ageing on microstructure evolution and mechanical properties of a 2024-T351 aluminium alloy,International Journal of Fatigue 107 (2018) 60-71.

[7] V. Hutsaylyuk, L. Snieżek, M. Chausov, J. Torzewski, A. Pylypenko, M. Wachowski, Cyclic deformation of aluminium alloys after the preliminary combined loading, Engineering Failure Analysis 69 (2016) 66-76, doi:10.1016/j.engfailanal.2016.07.002

[8] H. Mayer, R. Schuller, M.Fitzka, Fatigue of 2024-T351 aluminium alloy at different load ratios up to 10 10 cycles, International Journal of Fatigue 57 (2013) 113-119, doi:10.1016/j.ijfatigue.2012.07.013

[9] S. Khan, A. Vyshnevskyy, J. Mosler, Low cycle lifetime assessment of Al2024 alloy, International Journal of Fatigue 32(8) (2010) 1270-1277, doi:10.1016/j.ijfatigue.2010.01.014

[10]A. Gautam, P.K. Sarkar, R. Jangid, K.P. Ajit, Ductile and Fatigue Behaviour Estimation of Lightweight High-Strength Al 2024, Materials Today: Proceedings 5(2) (2018) 7873-7881, doi:10.1016/j.matpr.2017.11.468

[11]P. Kulkarni, Evaluation of Mechanical Properties of AL 2024 Based Hybrid Metal Composites, IOSR Journal of Mechanical and Civil Engineering 12(5) (2015) 108-122, doi:10.9790/1684-1254108122

[12]Jianzhong Zhou, Suqiang Xu, Shu Huang, XiankaiMeng, Jie Sheng, Haifeng Zhang, Jing Li,Yunhui Sun and Emmanuel Agyenim Boateng, Tensile Properties and Microstructures of a 2024-T351 Aluminum Alloy Subjected to Cryogenic Treatment, Metals 6(11) (2016 2796 doi:10.3390/met6110279

[13]Information on www.nordtechno.com/files/Franke_GK2011_en.pdf